Uncovering spatially resolved 6PPDQ metabolism in rainbow trout fry with nano-DESI mass spectrometry imaging

Nicholas Woytowich[1,2], Catherine Roberts[3], Phillip Ankley[3], Markus Brinkmann[3,4,5], Erik T. Krogh[1,2], Kyle D. Duncan[1,2*]

[1] Department of Chemistry, Vancouver Island University, Nanaimo, BC, Canada
[2] Department of Chemistry, University of Victoria, Victoria, BC, Canada
[3] Toxicology Centre, University of Saskatchewan, Saskatoon, SK, Canada
[4] Global Institute for Water Security (GIWS), Saskatoon, SK, Canada
[5] School of Environment and Sustainability (SENS), University of Saskatchewan, Saskatoon, SK, Canada

Keywords: mass spectrometry imaging, ambient ionization, nano-DESI, spatial metabolomics, toxicology, tire wear toxicants

*Corresponding author:

Dr. Kyle Duncan
Kyle.Duncan@viu.ca
Department of Chemistry
Vancouver Island University
900 Fifth Street, Nanaimo
BC, Canada, V9R 5S5

Abstract:

N-(1,3-Dimethylbutyl)-*N*'-phenyl-*p*-phenylenediamine quinone (6PPDQ) is an emerging tire-derived contaminant that poses a critical environmental risk to select salmonids. However, the mechanisms of 6PPDQ toxicity are currently unresolved. While species-specific metabolomic effects of 6PPDQ exposure have been explored, to our knowledge no studies have investigated the *in situ* spatial distribution of 6PPDQ and 6PPDQ biotransformation products in salmonids. Herein, we employ nanospray desorption electrospray ionization (nano-DESI) mass spectrometry imaging (MSI) to visualize 6PPDQ metabolism in 6-week post-hatch rainbow trout fry exposed to a 0.61 µg/L time-weighted concentration of 6PPDQ for 96 hours, as well as control fry. These data provide the first spatial mapping of 6PPDQ metabolism in fishes. 6PPDQ was not observed in any fish tissues; however, the primary 6PPDQ biotransformation product, hydroxylated 6PPDQ, was found to localize in the liver and gut of exposed fry. Additionally, interrogation of non-targeted nano-DESI spatial metabolomics revealed an accumulation of free fatty acids in the central nervous system of exposed fry. Overall, this study uncovers spatially resolved 6PPDQ metabolism in exposed fishes and explores the disparate localization of endogenous metabolites disrupted by 6PPDQ exposure.

Introduction:

N-(1,3-Dimethylbutyl)-*N*'-phenyl-*p*-phenylenediamine quinone (6PPDQ) is an environmental transformation product of the antioxidant tire rubber additive 6PPD, and has been shown to cause species-specific acute toxicity at ultra-trace levels.[1] Identified in 2021 by Tian *et al*., 6PPDQ is responsible for the mass pre-spawn mortality events and associated urban runoff mortality syndrome (URMS) observed in Pacific Northwest Coho salmon (*Oncorhynchus kisutch*).[1] Given its predicted global generation,[2] ubiquity in urban waterways,[3–6] and markedly low 24-hour median lethal concentration (LC_{50}) of 95 ng/L in adult Coho salmon,[7] 6PPDQ is a toxicant of great and widespread concern. Environmental concentrations frequently exceed LC_{50} values and pose a risk to other related salmonids, including white-spotted char (*Salvelinus leucomaenis pluvius*, 24-hour LC_{50} 0.51µg/L)[8], brook trout (*Salvelinus fontinalis*, 24-hour LC_{50} 0.59 µg/L)[9], and rainbow trout (*Oncorhynchus mykiss*, 24-hour LC_{50} 1.96 µg/L)[9], while other fishes, such as the phylogenetically close Arctic char (*Salvelinus alpinus,* 24-hour LC_{50} > 14.2 µg/L)[9] were insensitive to concentrations far exceeding those measured in the environment.[3]

Presently, the mechanism of toxicity observed in salmonids is unknown. The disparate toxicological responses among sensitive and insensitive species and between life stages of the same species are important in elucidating 6PPDQ toxicity. Further, the ability of salmonids to biotransform 6PPDQ likely plays an important role in its toxicity.[10–12] Additionally, factors such as exposure concentration and duration, species, and life stage are of interest when considering the abundance and types of 6PPDQ biotransformation products (bioTPs). For example, the presence of Phase I mono-hydroxylated 6PPDQ bioTPs is well characterized among various species.[13] However, less sensitive species exhibit an increase variety and abundance of Phase II bioTPs, including 6PPDQ-*O*-glucuronides, which may help to explain the difference in their sensitivity to 6PPDQ.[13] As such, the identification and relative concentration of bioTPs within various species and life stages is important to study. While sensitive and selective, conventional toxicological LC-MS metabolomics assays of rainbow trout cell lines,[14] extracted gall bladder bile liquid,[13] liver,[15] brain,[16] and whole-body homogenates[17] limit the observation of 6PPDQ metabolism in localized tissue subregions.

Herein, we used nanospray desorption electrospray ionization mass spectrometry imaging (nano-DESI MSI)[18] for *in situ* characterization of 6PPDQ and 6PPDQ bioTPs in rainbow trout fry. Mass spectrometry images were acquired at µm resolution for technical and biological replicates of 6-week post-hatch rainbow trout fry exposed to time-weighted average concentrations of 0.61 µg/L 6PPDQ for 96 hours, as well as control fry. To assess the impact of tissue matrix on 6PPDQ sensitivity, a spiked tissue mimetic model was used to estimate 6PPDQ limits of detection by nano-DESI MSI. Additionally, the use of a high-resolution mass spectrometer (HRMS) allows for the putative identification of metabolites in tissue. By coupling the nano-DESI MSI platform to a HRMS, it is possible to spatially resolve non-targeted metabolites. Localized changes in the abundance of these endogenous metabolites could help to elucidate impacted biological pathways and tissues perturbed by 6PPDQ exposure. Overall, this study simultaneously reveals the spatial accumulation 6PPDQ bioTPs *in situ* and provides a unique opportunity to uncover disparate localizations of exogenous and endogenous metabolites.

Experimental:

Fish samples and preparation:

Rainbow trout fry care, maintenance, and exposure are described previously.[19] All experiments involving animals were reviewed and approved by the University of Saskatchewan Animal Research Ethics Board (Animal Use Protocol 20220002). Prior to sectioning, fry were flash-frozen and stored at -80 °C. Whole fish were sectioned to 12 µm thickness using a cryostat (Leica CM 1850, Leica Microsystems Inc.) at -25 °C. Fry were sectioned along the sagittal plane to preserve morphological regions of interest and then thaw-mounted directly to regular glass microscope slides (Selectfrost, Fisher Scientific, Ottawa, ON). Slides were stored at -80 °C until MSI analysis.

Solvent preparation and Nano-DESI MSI:

MSI was performed on a custom-built platform, as previously outlined.[18,20,21] The nano-DESI solvent had 250 nM 6PPDQ-d_5 (100 µg/mL in ACN, HPC Chemicals, Atlanta, GA), 2 µM LysoPC 19:0, and 0.1% formic acid in 9:1 LC-MS Optima grade methanol (Fisher Scientific) in water (v/v). The nano-DESI solvent was supplied through a primary capillary at 0.5 µL min^{-1} *via* a syringe pump (KD Scientific 788180, KD LEGATO 180, Holliston MA). Tissue-mounted slides were placed onto the nano-DESI platform and the sample was moved at 40 µm s^{-1} along the x-axis and stepped in 150 µm increments along the y-axis. The nano-DESI platform was coupled to a Thermo Orbitrap Exploris 120, with ESI voltage set to 3.4kV and the MS inlet heated to 250 °C. MS^2 spectra were obtained for 6PPDQ, 6PPDQ-d_5, and OH-6PPDQ with a collision energy of 20 eV. Additionally, full scan (90-900 *m/z*) spectra were collected for non-targeted analysis. All experiments were performed in positive mode with a mass resolution of 120,000 (m/ Δm) at *m/z* 200. Thermo Fisher raw files were converted to centroided mzML files using MSConvert (Proteowizard),[22] and the ion images were generated from ion-2-image software.[23] Images were generated from the closest peak to the analyte mass, with an absolute mass tolerance window of 5 ppm. Pixel dimensions were calculated to be ~100 x 150 µm through vertical and lateral sample movement and the MS scan duty cycle.

Preparation of spiked tissue homogenates:

Mature Chinook salmon (*Oncorhynchus tshawytscha)* livers were obtained and flash-frozen prior to long-term storage at -20 °C. Approximately 1g of liver was added to a homogenizer microtube along with one 5-mm steel bead before homogenization at 4.0 m/s for 90 seconds. 100 µL aliquots of homogenate were transferred into 6 new microtubes containing one 1 mm zirconium oxide bead. A 100 µg/mL 6PPDQ standard (ACP Chemicals, Montreal, QC) was used to generate a calibration series, where 10 µL of the standard was spiked into the tissue homogenate aliquots. This resulted in final tissue concentrations of 0, 0.75, 1.50, 2.25, 3.00, and 3.75 µM. Following 6PPDQ spike addition, the 6 microtubes were homogenized again at 4.0 m/s for 30 seconds. 30 µL of spiked tissue homogenate was withdrawn from each microtube and pipetted directly into individual wells of a custom gelatin mold. The mold was stored at -80 °C for 1 hour before sectioning to 12 µm thickness.

Non-targeted MSI:

Non-targeted feature lists were generated from whole fish region-of-interest (ROI) masks for all tissue sections, using i2i with the following specifications: 5 ppm tolerance, 15% minimum pixel count, 5,000 minimum signal intensity, and a fold change of 2. Features within 5 ppm and appearing in at least five ion images were compiled to generate a comprehensive feature list. Signal intensities were extracted from whole-fish ROIs based on the comprehensive list. Average signal intensities

across the ROIs were obtained, and pixels containing signal intensities for the 5th and 95th percentiles were eliminated to remove artifacts and smooth data. MetaboAnalyst (version 6.0)[24] was used for spectral analysis of control and exposed bins. A volcano plot was generated, and significant features (p-value < 0.05) with a fold change (FC) > 2 were extracted and compiled with additional features of interest. These features were putatively identified using Human Metabolome Database (HMDB) for the $[M + H]^+$, $[M + Na]^+$, $[M + K]^+$ adducts and a mass tolerance of 10 ppm. Putative annotations of metabolites of interest were confirmed through on-tissue MS^2 using the nano-DESI platform. $[M + H]^+$ ions were confirmed for 6PPDQ and its bioTPs in positive mode, and $[M-H]^-$ ions were confirmed for fatty acids in negative ion mode with 2.4kV ESI potential (Table S2), with a ramping collision energy of 15-50 eV for all.

Results and Discussion:

Nano-DESI MSI of 6PPDQ and 6PPDQ biotransformation products:

To investigate 6PPDQ metabolism *in situ*, nano-DESI MSI was performed on whole-body thin tissue sections of 6PPDQ-exposed and control rainbow trout fry, with targeted selected ion monitoring (SIM) and MS^2 scans for 6PPDQ and several previously reported bioTPs.[10,13,17] Ion images in Figure 1 reveal that no 6PPDQ was detected in exposed or control fry. However, the phase I bioTP, monohydroxylated 6PPDQ (OH-6PPDQ), was found to localize in the liver and surrounding organs of exposed fry (Figure 1A). The identity of OH-6PPDQ was verified with on-tissue MS^2, where observed product ions represent the partial loss of an alkyl chain and retention of the hydroxy group at *m/z* 272.1154 and 259.1083, respectively.[1,14] OH-6PPDQ was not observed in control fry tissue (Figure 1A, 1B, 1C). Hydroxylation is thought to primarily occur in the para-position of the phenyl moiety;[14,25] however, the less abundant alkyl hydroxylation has been linked to site-specific[11] and regio-specific[12] toxicity. Unfortunately, it is not currently possible to distinguish OH-6PPDQ isomers with nano-DESI MSI and all data represent cumulative isomer classes. Our data suggest that 6PPDQ is present in the fry tissue at lower levels than OH-6PPDQ, and that OH-6PPDQ accumulates in the liver and surrounding organs in the exposed fry. Given the high ionizability and MS sensitivity previously observed for 6PPDQ, it is possible that 6PPDQ is bioconjugating or rapidly metabolizing to concentrations below the limit of detection for nano-DESI.

A tissue mimetic model was created from adult Chinook liver and was spiked with increasing concentrations of 6PPDQ to estimate nano-DESI MSI limit of detection (LOD) for 6PPDQ in tissue. The data were analyzed by extracting ROI mean intensities for 6PPDQ and the 6PPDQ-d_5 internal standard added to the nano-DESI solvent. This spiked tissue mimetic model allowed the construction of a tissue matrix-matched calibration curve for 6PPDQ in salmonid liver (Figure 2B). From the calibration curve, an on-tissue LOD for 6PPDQ was estimated to be 1 µM, which corresponds to ~0.3 µg/g of tissue. Interestingly, LODs for 6PPDQ in the nano-DESI solvent while not on tissue, such as droplet recovery on glass slide, were found to be several orders of magnitude lower, with picomolar concentrations detected (Figure S1). Additionally, low nanomolar (50 nM) concentrations of 6PPDQ-d_5 in the nano-DESI solvent were found completely suppressed in certain tissue regions of the rainbow trout fry (Figure S2). Altogether, the heavy signal suppression observed for 6PPDQ-d_5 in the nano-DESI solvent and high on-tissue 6PPDQ LODs may indicate more than just strong competition for ionization or other ESI matrix effects; it is possible that 6PPDQ is rapidly reacting or binding to biomolecules present within the liver tissue.

The localization of OH-6PPDQ to the liver, gut, and other proximal tissue (Figure 1A) is interesting, as cytochrome P450 (CYP450) enzymes are known to metabolize xenobiotics in the liver and are of interest in 6PPDQ metabolism.[26] Previously described experiments with RTL-W1 cell lines[14] and rainbow trout liver cells[11] cultured with 6PPDQ and several characterized CYP450 inhibitors uncovered non-descript CYP450 enzymes responsible for phase I 6PPDQ metabolism. In fish, major CYP450 activity occurs hepatically.[26] However, species-specific CYP450 activity has been studied extensively and extrahepatic activity has been observed in various organs of rainbow trout, including the gut, heart, and spleen.[26] Given the extent of 6PPDQ bioTPs in extrahepatic organs, the origin of 6PPDQ metabolism is ambiguous. It is unclear whether we are observing liver-derived 6PPDQ bioTPs perfusing into nearby tissues, or if 6PPDQ metabolism is occurring simultaneously in many organs.[13] It should be noted that there is still uncertainty about whether 6PPDQ or metabolic bioactivation are the main drivers of toxicity in rainbow trout.[11,12,25,27] For example, 6PPDQ without observable bioTPs has been shown to decouple mitochondrial respiration in RTgill-W1 cell lines,[27] but site-specific hydroxylation of OH-6PPDQ has also been shown to induce toxicity in fish.[11,12] Altogether, our data demonstrate that the primary bioTP, OH-6PPDQ, is present at higher levels than 6PPDQ in exposed fry, and that OH-6PPDQ is exclusively detected in the liver and surrounding organs.

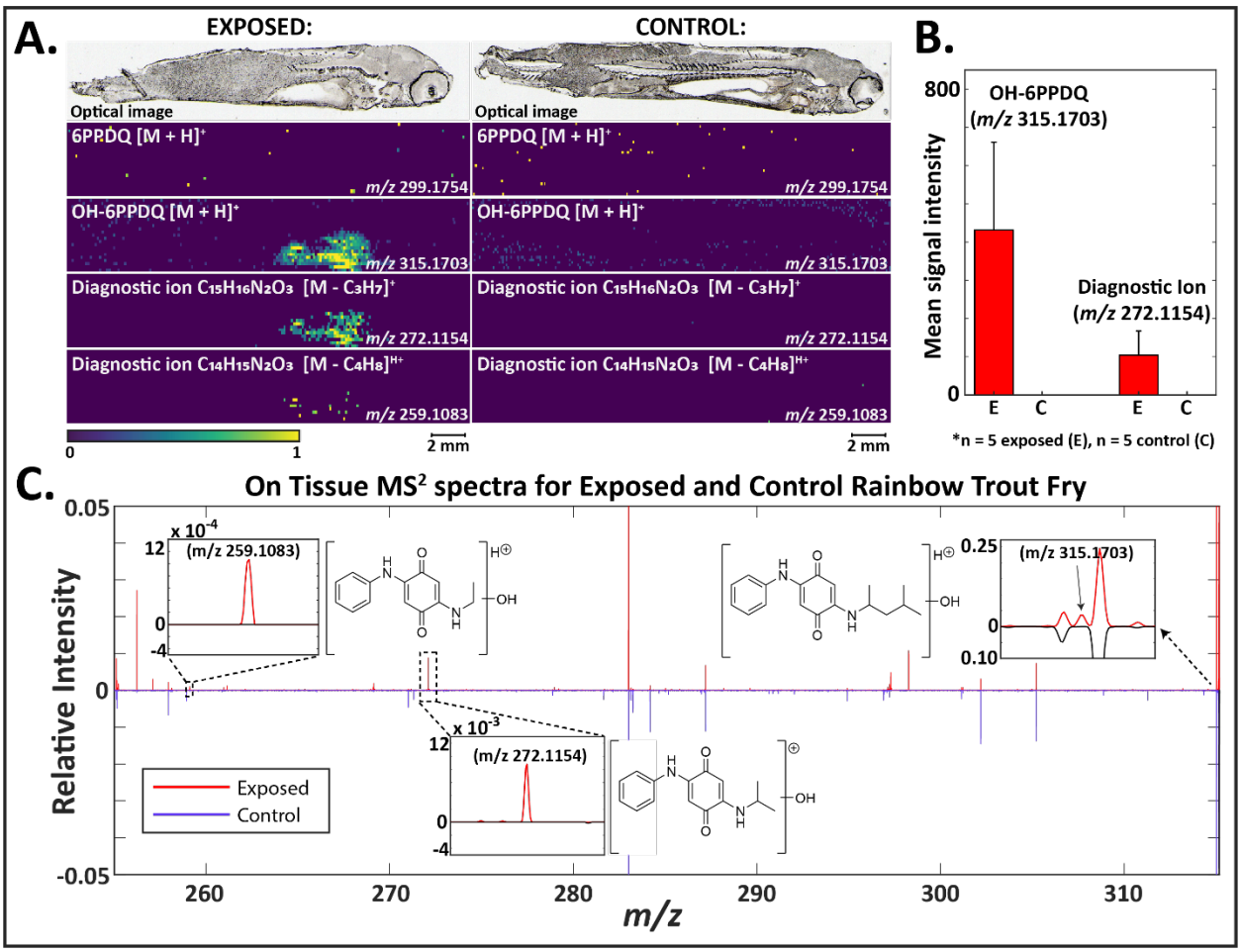

Figure 1. **A.** Optical image and corresponding ion images of 6PPDQ (SIM), OH-6PPDQ (MS^2), and two diagnostic ions of OH-6PPDQ, m/z 272.1161 and 259.1083 (MS^2). 6PPDQ SIM ion images were normalized to 6PPDQ-d_5 internal standard. MS^2 ion images for OH-6PPDQ and diagnostic ions were normalized to TIC. All ion images display relative color bar scaling with increasing pixel brightness relative to signal intensity. Scale bar 2 mm. **B.** ROI analysis for the OH-6PPDQ bioTP and most prevalent diagnostic fragment ion (m/z 272.1154) in exposed (E) and control (C) rainbow trout fry. Average intensities were normalized across 3 biological replicates with 3 technical replicates for one fry in each exposure bin (total n = 5 exposed, n = 5 control); normalized to the MS^2 filter TIC. Error bars represent one standard deviation. **C.** On tissue MS^2 spectra of an averaged line scan of exposed (top, red) and control (inverted bottom, blue) rainbow trout fry with highlighted precursor and diagnostic ion peaks and their associated structures. Relative intensities are displayed as a fraction of the largest intensity in the spectrum.

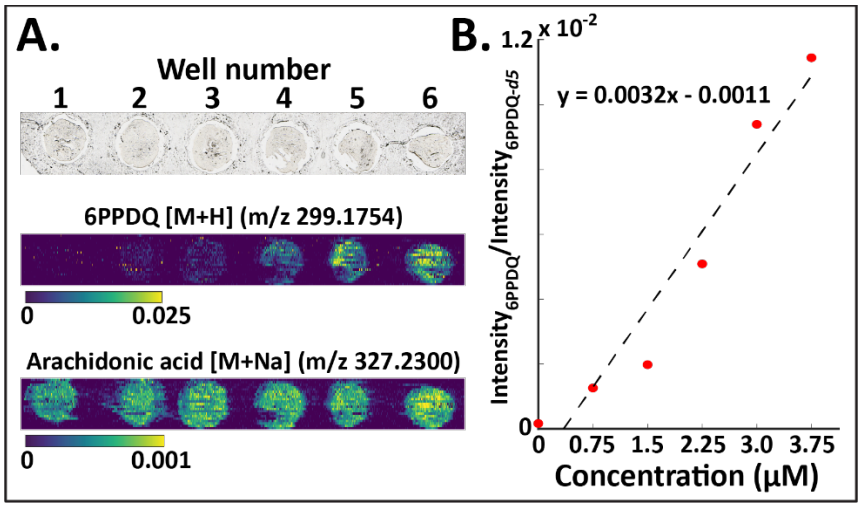

Figure 2. **A.** Optical image of Chinook salmon liver homogenate imbedded in gelatin with corresponding TIC-normalized ion images for the spiked 6PPDQ calibration curve (SIM) and Arachidonic acid (full-scan). Relative color bar scaling. **B.** Spike recovery calibration curve for 6PPDQ generated from ROI mean signal intensities and normalized to 6PPDQ-d_5 internal standard in the nano-DESI solvent.

Non-targeted spatial metabolomics of 6PPDQ exposed fry

Non-targeted nano-DESI MSI can help to elucidate biomolecular mechanisms of 6PPDQ toxicity by uncovering spatially resolved perturbations in endogenous metabolites. Using full scan data collected between *m/z* 95-900, a comprehensive feature list was compiled for all peaks found to be on-tissue in the imaged exposed and control fry. From these 711 molecular features, a volcano plot was generated, which revealed 52 upregulated and 14 downregulated metabolites for exposed and control fry (Figure 3A). Analysis of the tentatively identified molecular features uncovered a total of seven long-chain polyunsaturated fatty acids (LC-PUFAs) accumulated in the exposed fry as both $[M + Na]^+$ (Figure 3B, 3C, S4) and $[M + K]^+$ adducts (Figure S5). Interestingly, all of the identified LC-PUFAs were found to accumulate in the central nervous system of the exposed fish (Figure 3C). 6PPDQ has been implicated in disruption of the blood-brain barrier (BBB),[16,28] which has been associated with neuronal dysfunction, neuroinflammation, and death,[29–31] and may help to explain the increase in free LC-PUFAs observed in the central nervous system of exposed fry. The specific accumulated LC-PUFAs were docosahexaenoic acid (DHA), arachidonic acid (ARA), eicosapentaenoic acid (EPA), docosapentaenoic acid (DPA), docosatetraenoic acid (DTA), tetracosahexaenoic acid (THA), and tetracosapenaenoic acid (TPA). Identities of these metabolites were confirmed with on-tissue MS^2 in negative mode for the $[M - H]^-$ adduct (Table S1). TIC-normalized signal intensities were extracted from whole-fish and brain ROIs from MSI, revealing an increase in LC-PUFAs across whole fish in the exposure group (Figure 3C). Interestingly, only DHA, DPA, EPA and ARA displayed significant abundance in the brain versus whole-body (Figure 3C). LC-PUFAs are highly abundant in salmonids, and by weight, DHA, DPA, EPA, and ARA contribute over 30% of the total free fatty acid profile in the brains of wild, mature rainbow trout.[32] Given that LC-PUFAs cannot be directly biosynthesized in fish and require desaturation and chain elongation of essential fatty acids,[33] we also investigated spatially resolved accumulation of LC-PUFA containing biomolecules that can act as a source of free LC-PUFA upon enzymatic liberation.[21] Specifically, whole fish and brain ROI intensities were extracted for putatively identified LC-PUFA containing phosphatidylcholines (PC), lysophosphatidylcholines (LysoPC), and monoacylglycerols (MAG). Surprisingly, no significant differences were observed between exposed and control fry for putatively identified LC-PUFA bearing lipids (Figure S6, S7, and S8), potentially suggesting another route for LC-PUFA accumulation in exposed fry. ROI mean intensities were also extracted for putatively identified LC-PUFA containing acylcarnitines, with no significance observed between exposed and control fry (Figure S9). To summarize, the non-targeted nano-DESI MSI data identified accumulation of LC-PUFAs in the central nervous system of 6PPDQ-exposed fry, without significant changes to the levels of larger LC-PUFA containing lipids and acylcarnitines.

This study provides the first spatially resolved distribution of 6PPDQ metabolism in exposed fish. The lack of observable 6PPDQ may indicate that 6PPDQ rapidly metabolizes into its bioTPs. OH-6PPDQ was found to localize exclusively to the liver, gut, and other spatially proximal tissues. Given the extent of OH-6PPDQ accumulation in extrahepatic organs, it is unclear whether 6PPDQ metabolism is occurring simultaneously in many organs or if liver derived OH-6PPDQ is perfusing into them. Additionally, non-targeted spatial metabolomics revealed the accumulation of free LC-PUFAs in the central nervous system. LC-PUFA bearing lipids and acylcarnitines were assessed as potential sources of these free LC-PUFAs, but significant differences in abundance were not observed between exposed and control fry suggesting another route for LC-PUFA genesis. Further, perturbations to LC-PUFAs are found to occur in different regions of the fish than observed 6PPDQ metabolism, indicating that disruption of biological pathways can occur independently from major bioTP accumulation.

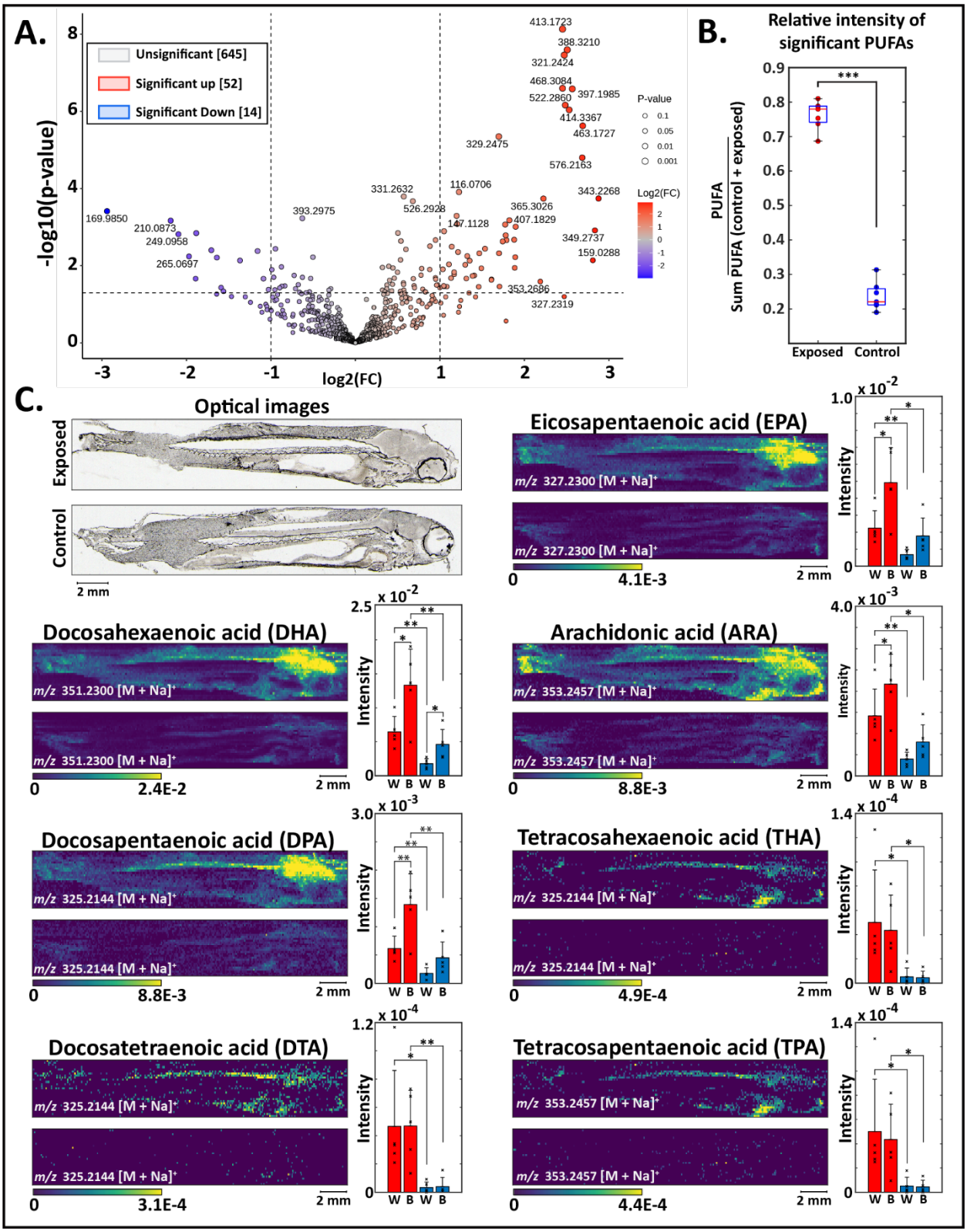

Figure 3. **A.** Volcano plot for non-targeted analysis comparing exposed (n=5 images, 3 biological replicates, 3 technical replicates of one fish) and control (n=5 images, 3 biological replicates, 3 technical replicates of one fish) rainbow trout fry. TIC normalized intensities were extracted from whole fish regions-of-interest, with the removal of 5th and 95th percentile intensities. **B.** Box and whisker plot of seven long-chain polyunsaturated fatty acids (LC-PUFAs) upregulated in exposed

rainbow trout fry. Signal intensity is displayed as a fraction of total signal intensity (relative to total signal intensity) with the removal of the 5th and 95th percentile intensities. *** *p*-value < 0.001. **C.** Optical images and corresponding TIC normalized ion images and intensity analysis of seven LC-PUFAs in exposed (top/red) and control (bottom/blue) rainbow trout fry. Exposed and control ion images conserve absolute color bar scaling for specific lipids of interest. Mean intensities were pulled from regions-of-interest for the whole fish (W) and in the brain (B) and averaged across replicates. Error bars represent one standard deviation, and p-values are indicated as: * *p*-value < 0.05, ** *p*-value < 0.01.

Conflicts of interest: The authors have no conflicts of interest to declare.

Acknowledgements: The authors graciously acknowledge the ongoing support of graduate students and infrastructure from Vancouver Island University, the University of Victoria, and the Canadian Foundation for Innovation (Projects 32238 and 43810). This work was supported by funding provided by the NSERC Discovery Grant program (KDD RGPIN-202203696; ETK RGPIN-2022-05349) and the BC Salmon Restoration and Innovation Fund (BCSRIF_2022_389). This project was supported partially by a financial contribution from Fisheries and Oceans Canada.

Associated content:

Data availability statement: Data is available upon reasonable request to the corresponding author.

References:

(1) Tian, Z.; Zhao, H.; Peter, K. T.; Gonzalez, M.; Wetzel, J.; Wu, C.; Hu, X.; Prat, J.; Mudrock, E.; Hettinger, R.; Cortina, A. E.; Biswas, R. G.; Kock, F. V. C.; Soong, R.; Jenne, A.; Du, B.; Hou, F.; He, H.; Lundeen, R.; Gilbreath, A.; Sutton, R.; Scholz, N. L.; Davis, J. W.; Dodd, M. C.; Simpson, A.; McIntyre, J. K.; Kolodziej, E. P. A Ubiquitous Tire Rubber–Derived Chemical Induces Acute Mortality in Coho Salmon. *Science* **2021**, *371* (6525), 185–189. https://doi.org/10.1126/science.abd6951.

(2) Hu, X.; Zhao, H. N.; Tian, Z.; Peter, K. T.; Dodd, M. C.; Kolodziej, E. P. Transformation Product Formation upon Heterogeneous Ozonation of the Tire Rubber Antioxidant 6PPD (*N* -(1,3-Dimethylbutyl)- *N* '-Phenyl- *p* -Phenylenediamine). *Environ. Sci. Technol. Lett.* **2022**, *9* (5), 413–419. https://doi.org/10.1021/acs.estlett.2c00187.

(3) Challis, J. K.; Popick, H.; Prajapati, S.; Harder, P.; Giesy, J. P.; McPhedran, K.; Brinkmann, M. Occurrences of Tire Rubber-Derived Contaminants in Cold-Climate Urban Runoff. *Environ. Sci. Technol. Lett.* **2021**, *8* (11), 961–967. https://doi.org/10.1021/acs.estlett.1c00682.

(4) Jaeger, A.; Monaghan, J.; Tomlin, H.; Atkinson, J.; Gill, C. G.; Krogh, E. T. Intensive Spatiotemporal Characterization of the Tire Wear Toxin 6PPD Quinone in Urban Waters. *ACS EST Water* **2024**, *4* (12), 5566–5574. https://doi.org/10.1021/acsestwater.4c00614.

(5) Helm, P. A.; Raby, M.; Kleywegt, S.; Sorichetti, R. J.; Arabian, G.; Smith, D.; Howell, E. T.; Thibeau, J. Assessment of Tire-Additive Transformation Product 6PPD-Quinone in Urban-Impacted Watersheds. *ACS EST Water* **2024**, *4* (4), 1422–1432. https://doi.org/10.1021/acsestwater.3c00589.

(6) Cao, G.; Wang, W.; Zhang, J.; Wu, P.; Zhao, X.; Yang, Z.; Hu, D.; Cai, Z. New Evidence of Rubber-Derived Quinones in Water, Air, and Soil. *Environ. Sci. Technol.* **2022**, *56* (7), 4142–4150. https://doi.org/10.1021/acs.est.1c07376.

(7) Tian, Z.; Gonzalez, M.; Rideout, C. A.; Zhao, H. N.; Hu, X.; Wetzel, J.; Mudrock, E.; James, C. A.; McIntyre, J. K.; Kolodziej, E. P. 6PPD-Quinone: Revised Toxicity Assessment and

Quantification with a Commercial Standard. *Environ. Sci. Technol. Lett.* **2022**, *9* (2), 140–146. https://doi.org/10.1021/acs.estlett.1c00910.
(8) Hiki, K.; Yamamoto, H. The Tire-Derived Chemical 6PPD-Quinone Is Lethally Toxic to the White-Spotted Char *Salvelinus leucomaenis Pluvius* but Not to Two Other Salmonid Species. *Environ. Sci. Technol. Lett.* **2022**, *9* (12), 1050–1055. https://doi.org/10.1021/acs.estlett.2c00683.
(9) Brinkmann, M.; Montgomery, D.; Selinger, S.; Miller, J. G. P.; Stock, E.; Alcaraz, A. J.; Challis, J. K.; Weber, L.; Janz, D.; Hecker, M.; Wiseman, S. Acute Toxicity of the Tire Rubber-Derived Chemical 6PPD-Quinone to Four Fishes of Commercial, Cultural, and Ecological Importance. *Environ. Sci. Technol. Lett.* **2022**, *9* (4), 333–338. https://doi.org/10.1021/acs.estlett.2c00050.
(10) Grasse, N.; Seiwert, B.; Massei, R.; Scholz, S.; Fu, Q.; Reemtsma, T. Uptake and Biotransformation of the Tire Rubber-Derived Contaminants 6-PPD and 6-PPD Quinone in the Zebrafish Embryo (*Danio rerio*). *Environ. Sci. Technol.* **2023**, *57* (41), 15598–15607. https://doi.org/10.1021/acs.est.3c02819.
(11) Nair, P.; Barrett, H.; Tanoto, K.; Xie, L.; Sun, J.; Yang, D.; Yao, H.; Song, D.; Peng, H. Structure and Toxicity Characterization of Alkyl Hydroxylated Metabolites of 6PPD-Q. ChemRxiv October 30, 2024. https://doi.org/10.26434/chemrxiv-2024-s5rhc.
(12) Li, R.; Barrett, H.; Nair, P.; Wang, M.; Xie, L.; Peng, H. Enantioselectivity in Metabolism and Toxicity of 6PPD-Quinone in Salmonids. ChemRxiv November 4, 2024. https://doi.org/10.26434/chemrxiv-2024-87hn7.
(13) Montgomery, D.; Ji, X.; Cantin, J.; Philibert, D.; Foster, G.; Selinger, S.; Jain, N.; Miller, J.; McIntyre, J.; de Jourdan, B.; Wiseman, S.; Hecker, M.; Brinkmann, M. Interspecies Differences in 6PPD-Quinone Toxicity Across Seven Fish Species: Metabolite Identification and Semiquantification. *Environ. Sci. Technol.* **2023**, *57* (50), 21071–21079. https://doi.org/10.1021/acs.est.3c06891.
(14) Ankley, P. J.; da Silva, F. C. Jr.; Montgomery, D.; Schultz, M.; Ed S. Krol; Hecker, M.; Brinkmann, M. Biotransformation of 6PPD-Quinone In Vitro Using RTL-W1 Cell Line. *Environ. Sci. Technol. Lett.* **2024**, *11* (7), 687–693. https://doi.org/10.1021/acs.estlett.4c00342.
(15) Di, S.; Xu, H.; Yu, Y.; Qi, P.; Wang, Z.; Liu, Z.; Zhao, H.; Jin, Y.; Wang, X. Environmentally Relevant Concentrations of S-6PPD-Quinone Caused More Serious Hepatotoxicity Than R-Enantiomer and Racemate in *Oncorhynchus mykiss*. *Environ. Sci. Technol.* **2024**, *58* (40), 17617–17628. https://doi.org/10.1021/acs.est.4c06357.
(16) Blair, S. I.; Barlow, C. H.; McIntyre, J. K. Acute Cerebrovascular Effects in Juvenile Coho Salmon Exposed to Roadway Runoff. *Can. J. Fish. Aquat. Sci.* **2021**, *78* (2), 103–109. https://doi.org/10.1139/cjfas-2020-0240.
(17) Ankley, P. J.; da Silva Junior, F. C.; Roberts, C.; Eriksson, A. N. M.; Kohlman, E.; Dubiel, J.; Hunnie, B.; Anderson-Bain, K.; Urrutia, R. M.; Hogan, N.; Giesy, J. P.; Krol, E.; Wiseman, S.; Hecker, M.; Brinkmann, M. Xenometabolome of Early-Life Stage Salmonids Exposed to 6PPD-Quinone. June 14, 2024. https://doi.org/10.1101/2024.06.12.598661.
(18) Lanekoff, I.; Heath, B. S.; Liyu, A.; Thomas, M.; Carson, J. P.; Laskin, J. Automated Platform for High-Resolution Tissue Imaging Using Nanospray Desorption Electrospray Ionization Mass Spectrometry. *Anal. Chem.* **2012**, *84* (19), 8351–8356. https://doi.org/10.1021/ac301909a.
(19) Roberts, C.; Kohlman, E.; Jain, N.; Amekor, M.; Alcaraz, A. J.; Hogan, N.; Brinkmann, M.; Hecker, M. Sub-Chronic and Acute Toxicity of 6PPD-Quinone to Early-Life Stage Rainbow Trout (*Oncorhynchus mykiss*). bioRxiv September 26, 2024, p 2024.09.25.614982. https://doi.org/10.1101/2024.09.25.614982.

(20) Duncan, K. D.; Sun, X.; Baker, E. S.; Dey, S. K.; Lanekoff, I. In Situ Imaging Reveals Disparity between Prostaglandin Localization and Abundance of Prostaglandin Synthases. *Commun. Biol.* **2021**, *4* (1), 966. https://doi.org/10.1038/s42003-021-02488-1.
(21) Nguyen, K.; Carleton, G.; Lum, J. J.; Duncan, K. D. Expanding Spatial Metabolomics Coverage with Lithium-Doped Nanospray Desorption Electrospray Ionization Mass Spectrometry Imaging. *Anal. Chem.* **2024**, *96* (46), 18427–18436. https://doi.org/10.1021/acs.analchem.4c03553.
(22) Chambers, M. C.; Maclean, B.; Burke, R.; Amodei, D.; Ruderman, D. L.; Neumann, S.; Gatto, L.; Fischer, B.; Pratt, B.; Egertson, J.; Hoff, K.; Kessner, D.; Tasman, N.; Shulman, N.; Frewen, B.; Baker, T. A.; Brusniak, M.-Y.; Paulse, C.; Creasy, D.; Flashner, L.; Kani, K.; Moulding, C.; Seymour, S. L.; Nuwaysir, L. M.; Lefebvre, B.; Kuhlmann, F.; Roark, J.; Rainer, P.; Detlev, S.; Hemenway, T.; Huhmer, A.; Langridge, J.; Connolly, B.; Chadick, T.; Holly, K.; Eckels, J.; Deutsch, E. W.; Moritz, R. L.; Katz, J. E.; Agus, D. B.; MacCoss, M.; Tabb, D. L.; Mallick, P. A Cross-Platform Toolkit for Mass Spectrometry and Proteomics. *Nat. Biotechnol.* **2012**, *30* (10), 918–920. https://doi.org/10.1038/nbt.2377.
(23) Lilija, J.; Duncan, K.; Lanekoff, I.; Ion-to-Image, i2i, a Mass Spectrometry Imaging Data Analysis Platform for Continuous Ionization Techniques.Anal. Chem. **2023**, 95, 31, 11589–11595. https://pubs.acs.org/doi/full/10.1021/acs.analchem.3c01615.
(24) Pang, Z.; Lu, Y.; Zhou, G.; Hui, F.; Xu, L.; Viau, C.; Spigelman, A. F.; MacDonald, P. E.; Wishart, D. S.; Li, S.; Xia, J. MetaboAnalyst 6.0: Towards a Unified Platform for Metabolomics Data Processing, Analysis and Interpretation. *Nucleic Acids Res.* **2024**, *52* (W1), W398–W406. https://doi.org/10.1093/nar/gkae253.
(25) Nair, P.; Sun, J.; Xie, L.; Kennedy, L.; Kozakiewicz, D.; Kleywegt, S.; Hao, C.; Byun, H.; Barrett, H.; Baker, J.; Monaghan, J.; Krogh, E.; Song, D.; peng, hui. Synthesis and Toxicity Evaluation of Tire Rubber-Derived Quinones. June 20, 2023. https://doi.org/10.26434/chemrxiv-2023-pmxvc.
(26) Sarasquete, C.; Segner, H. Cytochrome P4501A (CYP1A) in Teleostean Fishes. A Review of Immunohistochemical Studies. *Sci. Total Environ.* **2000**, *247* (2), 313–332. https://doi.org/10.1016/S0048-9697(99)00500-8.
(27) Mahoney, H.; da Silva Junior, F. C.; Roberts, C.; Schultz, M.; Ji, X.; Alcaraz, A. J.; Montgomery, D.; Selinger, S.; Challis, J. K.; Giesy, J. P.; Weber, L.; Janz, D.; Wiseman, S.; Hecker, M.; Brinkmann, M. Exposure to the Tire Rubber-Derived Contaminant 6PPD-Quinone Causes Mitochondrial Dysfunction In Vitro. *Environ. Sci. Technol. Lett.* **2022**, *9* (9), 765–771. https://doi.org/10.1021/acs.estlett.2c00431.
(28) Greer, J. B.; Dalsky, E. M.; Lane, R. F.; Hansen, J. D. Tire-Derived Transformation Product 6PPD-Quinone Induces Mortality and Transcriptionally Disrupts Vascular Permeability Pathways in Developing Coho Salmon. *Environ. Sci. Technol.* **2023**, *57* (30), 10940–10950. https://doi.org/10.1021/acs.est.3c01040.
(29) Obermeier, B.; Daneman, R.; Ransohoff, R. M. Development, Maintenance and Disruption of the Blood-Brain Barrier. *Nat. Med.* **2013**, *19* (12), 1584–1596. https://doi.org/10.1038/nm.3407.
(30) Hawkins, B. T.; Davis, T. P. The Blood-Brain Barrier/Neurovascular Unit in Health and Disease. *Pharmacol. Rev.* **2005**, *57* (2), 173–185. https://doi.org/10.1124/pr.57.2.4.
(31) Brooks, T. A.; Hawkins, B. T.; Huber, J. D.; Egleton, R. D.; Davis, T. P. Chronic Inflammatory Pain Leads to Increased Blood-Brain Barrier Permeability and Tight Junction Protein Alterations. *Am. J. Physiol.-Heart Circ. Physiol.* **2005**, *289* (2), H738–H743. https://doi.org/10.1152/ajpheart.01288.2004.

(32) Tocher, D. R.; Harvie, D. G. Fatty Acid Compositions of the Major Phosphoglycerides from Fish Neural Tissues; (N−3) and (N−6) Polyunsaturated Fatty Acids in Rainbow Trout (*Salmo gairdneri*) and Cod (*Gadus morhua*) Brains and Retinas. *Fish Physiol. Biochem.* **1988**, *5* (4), 229–239. https://doi.org/10.1007/BF01874800.
(33) Zhang, Z.; Miar, Y.; Huyben, D.; Colombo, S. M. Omega-3 Long-Chain Polyunsaturated Fatty Acids in Atlantic Salmon: Functions, Requirements, Sources, de Novo Biosynthesis and Selective Breeding Strategies. *Rev. Aquac.* **2024**, *16* (3), 1030–1041. https://doi.org/10.1111/raq.12882.